Local order measurement in SnGe alloys and monolayer Sn films on Si with reflection electron energy loss spectrometry

Selmer S. Wong, Gang He, Shouleh Nikzad,[a] Channing C. Ahn, and Harry A. Atwater
Thomas J. Watson Laboratory of Applied Physics, California Institute of Technology, Pasadena, California 91125

(Received 28 March 1994; accepted 12 November 1994)

Measurements of local order are demonstrated in Sn-containing alloys and epitaxial monolayer thickness films by analysis of extended-edge energy loss fine structure (EXELFS) data obtained by reflection electron energy loss spectrometry (REELS). These measurements of short-range order provide a complement to the chemical information obtained with REELS and long-range order obtained using reflection high energy electron diffraction. The results suggest that EXELFS measurements are practical for samples mounted on the growth manipulator in a molecular beam epitaxy chamber. Advantages and limitations of reflection EXELFS are discussed. © *1995 American Vacuum Society.*

I. INTRODUCTION

The growth of thin films by molecular beam epitaxy and during-growth analysis has enabled synthesis of artificial structures with abrupt strain and composition profiles. Reflection high energy electron diffraction (RHEED) is well-suited to analysis of surface reconstructions and gives qualitative information about surface roughness. However, with the advent of growth of ever more abrupt layers and metastable layers, a practical method for *in situ* analysis of chemical composition and local order is also desirable. A good example is the observation of stable surface reconstructions induced by epitaxial growth of thin layers of boron on Si(100) and (111).[1] This suggests possibilities for monolayer doping and ordered alloy structures with unique electrical properties.[2]

In this article, we report an extended-edge energy loss fine structure (EXELFS) investigation of local order in Sn films on Si(100) and in Sn–Ge alloy films. Low-temperature (~330 °C) epitaxy of Si on Si(111) with a thin mediating layer of Sn on the surface has prompted investigations of structure and dynamics of surfactants, such as the tin-induced atomic structure of the $(2\sqrt{3}\times 2\sqrt{3})R30°$ reconstructed surface.[3] Moreover, the zero energy band gap of α-Sn,[4] which has a diamond structure, has prompted investigations of α-Sn/Ge quantum-well structures. When alloyed with germanium, α-SnGe is predicted to have a direct band gap in the range of 0.0–0.55 eV for tin concentrations of 0.2-0.6,[5] making such an alloy potentially useful in infrared optoelectronic applications. From a fundamental standpoint, Sn films on Si and Sn–Ge alloys are good systems for EXELFS analysis because the Sn $M_{4,5}$ edge energy loss cross section is relatively large. Previously, energy loss fine structure has been performed for epitaxial growth of Cu on Ag and was used to obtain information on strain relaxation during epitaxial growth.[6] Here we describe the use of similar methods to examine local order in semiconductor monolayer films and strained alloy layers.

We will discuss results of a study of local order in monolayer films of Sn on Si, and local order in SnGe alloys using reflection electron energy loss spectroscopy (REELS) and EXELFS analysis. REELS involves the spectral analysis of energy losses (due to core electron ionization) of RHEED electrons with energies ~30 keV from a sample surface with typical incidence angles of 0.5°–1.0°. The technical aspects of REELS are described in detail elsewhere.[7] Briefly, after impinging on the sample at grazing incidence, the scattered RHEED electrons strike a phosphorescent screen. A small aperture (~6 mm) drilled in the center of this screen allows a small component of the scattered beam to pass through the screen and into a set of energy-selecting slits, a magnetic prism spectrometer, and a photomultiplier tube for multichannel analysis. The reflection geometry of REELS gives it the advantage of use *during* growth, making possible real-time determinations of surface structure and composition on the atomic level during the initial, critical moments of deposition. By spectroscopically analyzing a small fraction of the scattered RHEED beam, it is possible to perform RHEED and REELS concurrently, yielding both surface structural and compositional information, with depth resolution of 15–20 Å, comparable to that of conventional surface analysis methods such as x-ray photoelectron spectroscopy and Auger electron spectroscopy, and with a detection limit of 5%–30% of a monolayer, depending on the particular core loss being investigated.[3,8] REELS has also been employed to obtain composition information for a variety of III–V, II–VI, and Si–Ge epitaxial systems.[9]

II. OVERVIEW OF EXELFS

The physical mechanism of EXELFS is analogous to the more well-known phenomenon of x-ray absorption fine structure (EXAFS). The incident beam particles are treated as waves. When an incident electron (e.g., a RHEED electron) impinges on a solid surface and ionizes an atom (hereafter denoted as the ''central'' atom), the outward-traveling scattered electron wave encounters neighbor atoms and has a finite probability of being scattered back by the neighbors toward the central atom (Fig. 1). The outgoing electron wave

[a]Also at the Microdevices Laboratory, Jet Propulsion Laboratory, Pasadena, CA 91109.

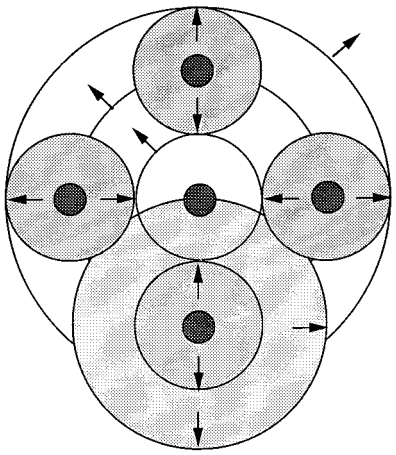

FIG. 1. EXELFS can be understood as a quantum-mechanical interference phenomenon between the outgoing electron wave and the incoming waves scattered back toward the central atom by near neighbor atoms.

interferes with the sum of the incoming waves, and it is this interference that gives rise to oscillations in the observed scattering intensity at a given energy loss. Thus EXELFS is unique to condensed matter, as it depends on the existence of shells of neighbor atoms at specific distances from the central atom. EXELFS is produced by the oscillation of the absorption coefficient due to neighbor atoms and is conventionally described mathematically by a function $\chi(k)$, the normalized absorption coefficient with respect to a free atom, for example, an atom in a dilute gas. Thus,

$$\chi(k)=\frac{\mu-\mu_0}{\mu_0},$$

where μ and μ_0 are the condensed matter and free atom absorption coefficients, respectively.

The functional form of $\chi(k)$ can be arrived at from physical considerations. The oscillations are expected to be proportional to $\sin(2kR+\delta)$, where k is the wave number of an incident electron of rest mass m and R is the distance between the central and neighbor atoms, and δ is a phase shift consisting of two components: $\delta(k)=\delta_l(k)+\varphi(k)$, where δ_l is the shift due to the central atom and φ is the shift due to the backscattering atom. The amplitude for scattering is obtained from application of Fermi's golden rule for the rate of the transition from the incident electron state $|\Psi_i\rangle$ to the final state $|\Psi_f\rangle$, using the Born approximation in the matrix element calculation, so that $|\Psi_i\rangle$ and $|\Psi_f\rangle$ are both plane wave states. The scattering intensity is proportional to the number of backscattering atoms, N, and has a $1/r^2$ dependence. Thermal and static disorder can be accounted for by a probability distribution term $\exp(-2k^2\sigma^2)$, where σ^2 is the mean square deviation of an atom in the material from its equilibrium position and contains both static (temperature-independent) and dynamic (temperature-dependent) components. The electron wave interference can remain coherent as long as it does not undergo too many scattering events; this can be taken into account by a mean free path term $\exp(-2R/\lambda)$. Combining the physical features gives

$$\chi(k)=\frac{m}{4\pi\hbar^2k}\sum_j \frac{N_j}{R_j^2} f_j(k,\pi)\sin[2kR_j+\delta_j(k)] \times\exp(-2k^2\sigma^2)\exp(-2R_j/\lambda),$$

where the summation is taken over all coordination shells, i.e., all groups of neighbor atoms at equivalent distances R_j from the central atom.

We consider the implications of the Born approximation, which assumes $\mathbf{q}\cdot\mathbf{r}\ll 1$, where q is the momentum transfer of the electron probe. For outer-shell electron ionization qr is small and the Born, or dipole, approximation holds reasonably well. For deeper core losses, on the other hand, q is significantly greater and, in principle, the dipole term $\mathbf{q}\cdot\mathbf{r}$ is no longer a good estimate of $\exp(i\mathbf{q}\cdot\mathbf{r})$ because higher-order multipole transitions become non-negligible. However, in practice, it is found that the main contribution to inelastic scattering comes from the dipole term, and higher-order transitions are in general detectable only when the dipole transition is forbidden or when the density of final states is high for a multipole transition.[10] Additionally, in our study the momentum transfers are small due to the high incident beam energy (25 keV) and grazing incidence geometry, lending further justification to use of the Born approximation.

It can be seen that the Fourier transform of $\chi(k)$ gives the radial probability distribution function (RDF), i.e., the probability of occurrence of neighbors at distances R_j from the central atom.

As with EXAFS and EXELFS in transmission mode, care must be taken in data reduction and analysis to obtain meaningful local order measurements. The fine structure oscillations must be sufficiently isolated from the raw data spectrum in order to obtain a high-quality, low-noise RDF. Insufficiently accurate background subtraction produces large-amplitude contributions in the low R region (0–2 Å) and may cause broadening and even shifts in the peaks corresponding to radial distances of near neighbors. To isolate the EXELFS in our analysis, we have modeled the large plasmon background with a power law and performed a rough background subtraction. Then, an estimation of the purely atomic core loss component, through which the EXELFS oscillation occurs, was done using a cubic polynomial spline fit. We have performed the spline fit in two different ways: (1) requiring that the values at the spline region "knots" meet and that the spline function derivatives match at these knots; and (2) relaxing the constraint that the endpoints at spline region boundaries must meet, and merely requiring that the derivatives match. We have found that method 1 gives a smoothly varying $\chi(k)$, free of discontinuities that may otherwise be produced by a background subtraction; however, in some cases method 2 is better able to follow the slowly varying second-derivative maxima and minima in the background, and thus remove these low-frequency components from the data which do not contribute to the EXELFS.

III. MONOLAYER Sn FILMS ON Si(100)

Tin-induced reconstructions of the Si(100) surface have been previously investigated by Ueda *et al.*[11] who have ob-

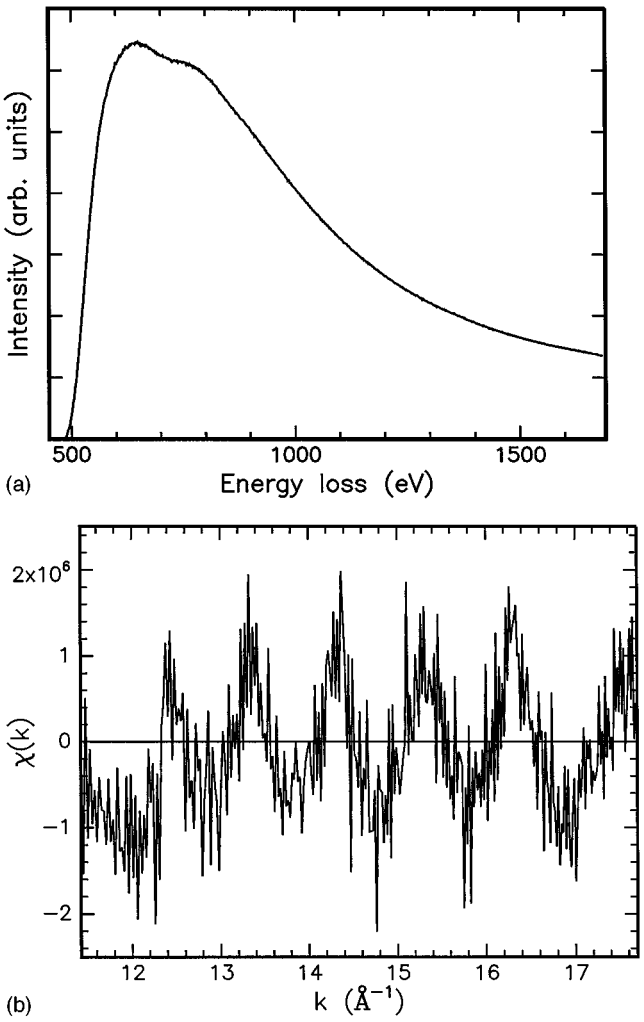

FIG. 2. (a) The background-subtracted Sn $M_{4,5}$ core loss intensity obtained from 1.9 ML of Sn on Si(100). The data region used for EXELFS analysis is 800–1660 eV. (b) The $\chi(k)$ function obtained after spline fit background subtraction of data in (a).

served (6×2), $c(4\times4)$, and (5×1) structures on clean Si(100) surfaces covered with thin layers of Sn. We have observed a new reconstruction, one with (3×1) periodicity as indicated by our RHEED data, on Si(100). The substrate was hydrogen-terminated via a hydrofluoric acid dip and prebaked *in situ* at 200 °C for 1 hour to desorb physisorbed hydrocarbons. Sn was then evaporated from a Knudsen-type effusion cell at a cell temperature of 1000 °C with a chamber base pressure of 5×10^{-10} Torr. The substrate temperature during growth was (200±20) °C, measured by a thermocouple in contact with the back of the substrate holder. Samples were annealed at 550 °C for several minutes after Sn deposition, and the (3×1) reconstructions were observed at 150–170 °C, after sample cooling. To investigate further the nature of the reconstruction, we have performed EXELFS analysis on this system, using the Sn $M_{4,5}$ edge intensity. The ionization cross section of Sn $M_{4,5}$ is relatively high, and the edge itself is well isolated from the nearest Si energy loss edge (i.e., Si K at 1839 eV) above the Sn $M_{4,5}$ threshold, making analysis relatively uncomplicated. The Sn M_2, M_3 and M_1 edges, with thresholds at 756, 714, and 884 eV, respectively, are superimposed on the EXELFS analysis region for the $M_{4,5}$ edge, but these edges contribute incoherently with respect to EXELFS oscillations for the $M_{4,5}$ and thus have no effect on our analysis. While interpretation of oscillations in $M_{4,5}$ edges is not well developed for the $M_{4,5}$ edges here, the RDF yields fairly accurate near-neighbor distances, as previous work[12] has shown that the phase shift contributions from the central atom and the backscattering atom have opposite effects and tend to cancel each other. Figure 2 shows the EXELFS data region used and the $\chi(k)$ function obtained from a 1.9 ML (monolayer) coverage of Sn on hydrogen-terminated Si(100). We note that the signal-to-background ratio is rather small due to the nature of core losses in the low energy loss regime; however, clear oscillations are apparent. Fourier transform of the $\chi(k)$ gives (without phase shift correction) a nearest-neighbor distance of (3.1 ±0.2) Å (Fig. 3). We did not deconvolute effects of multiple inelastic scattering from this transform. The film is thin enough so that single scattering dominated. Plasmon contributions reside primarily in the low k region; here, our Fourier transform window started at ~9 $Å^{-1}$ past the Sn $M_{4,5}$ threshold, well beyond the region where multiple scattering effects could become important. For electron scattering in the reflection geometry, these effects are larger than for the transmission geometry, thus broadening the nearest-neighbor peaks; however, the peak positions are not affected. For purposes of comparison, we have also obtained EXELFS measurements from the Si $L_{2,3}$ core edge intensity from a hydrogen-terminated, unreconstructed [i.e., (1×1)] Si(100) surface annealed for 2 h at 200 °C to desorb physisorbed hydrocarbons (see Fig. 4). The resulting RDF from Si(100) is superimposed in Fig. 3 on the Sn/Si RDF, showing a deviation from the bulk Si–Si distance. It is worth noting that this Si(100) RDF is consistent with the results of previous EXAFS and EXELFS studies of Si K edges,[13] despite the differences in backscattering and phase shifts associated with the K and $L_{2,3}$ edges. For a Sn coverage of 1.9 ML, this

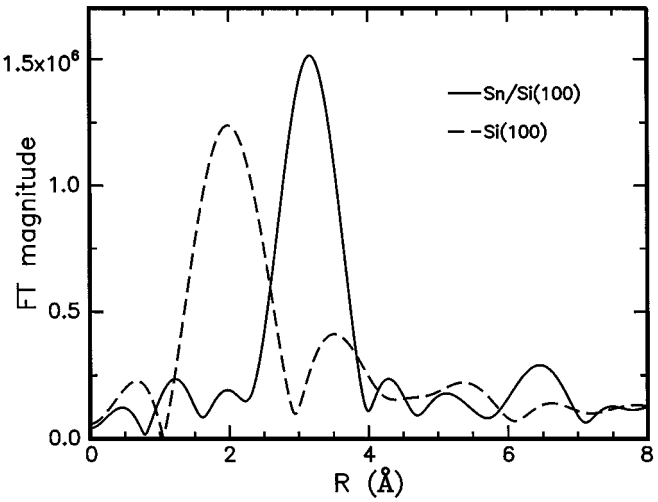

FIG. 3. The radial distribution function of 1.9 ML Sn/Si(100) (—) with nearest neighbor at 3.1 Å, after Fourier transform of Fig. 2(b). Superimposed is the RDF of Si(100) (- - -) with nearest neighbor at 2.0 Å. Neither RDF is phase shift corrected.

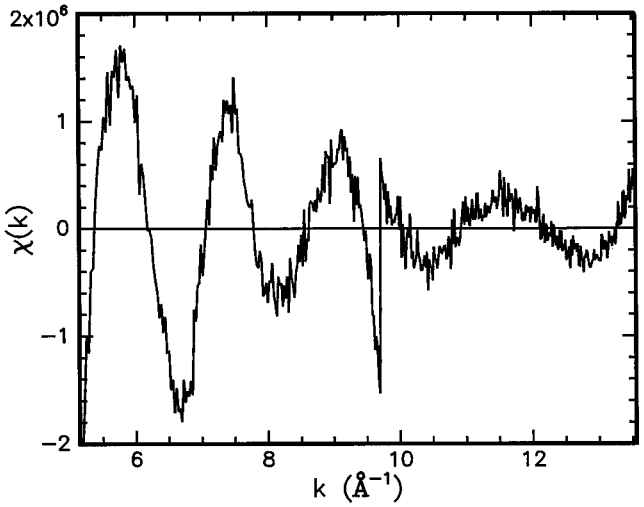

FIG. 4. The $\chi(k)$ function obtained from the Si $L_{2,3}$ core loss intensity from bare hydrogen-terminated Si(100). The sharp discontinuity is a result of relaxing a knot constraint in the background subtraction.

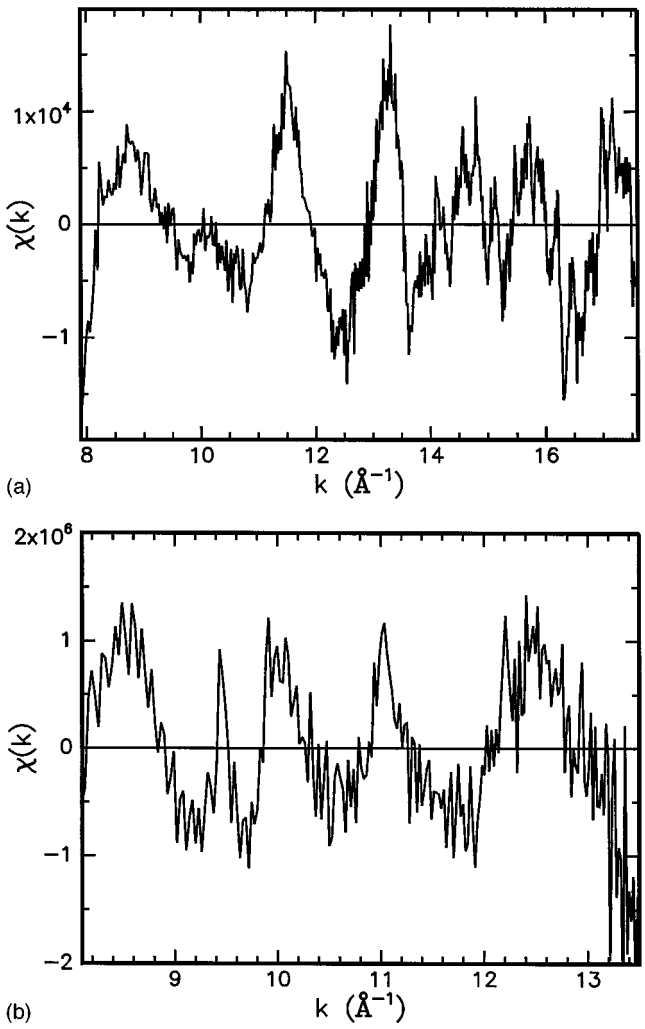

FIG. 5. The $\chi(k)$ functions from Sn $M_{4,5}$ edges from (a) $Sn_{0.01}Ge_{0.99}$ and (b) $Sn_{0.2}Ge_{0.8}$.

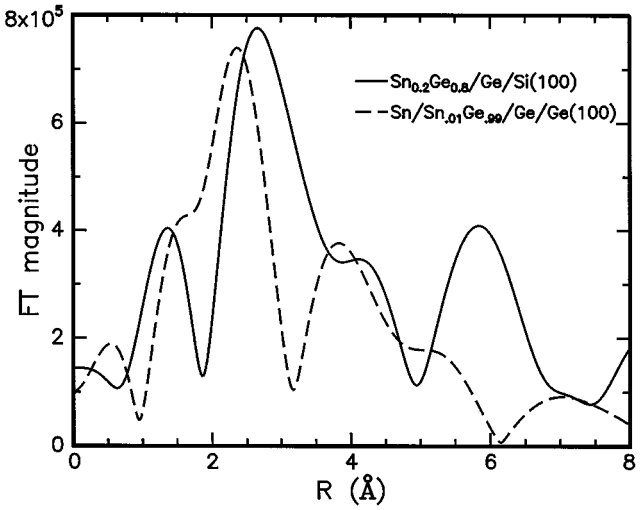

FIG. 6. The radial distribution functions of $Sn_{0.2}Ge_{0.8}$ (—) with nearest neighbors at 2.65 and 4.1 Å, and $Sn_{0.01}Ge_{0.99}$ (- - -) with nearest neighbors at 2.4 and 3.85 Å. Neither RDF is phase shift corrected.

radial probability function would represent a convolution of Sn–Si neighbors as well as Sn–Sn neighbors. A possible surface structure that is consistent with the measured coverage, the observed (3×1) periodicity and EXELFS-derived nearest-neighbor distance observed is a missing-row structure, in which the first monolayer of Sn is deposited on all Si surface sites, and the second monolayer is deposited so that there are two rows of Sn atoms for every three rows of Si atoms. This structure may also indicate the beginnings of faceting of the adsorbed Sn layer, in agreement with recent scanning tunneling microscope (STM) observations of faceting of metal atoms on semiconductor surfaces.[14]

IV. SnGe ALLOYS

REELS EXELFS analysis is also demonstrated in determining short-range order in epitaxial SnGe alloys. We have made REELS EXELFS measurements in the transmission electron microscope at room temperature on two such alloys. A strain-relieved 750 Å α-$Sn_{0.2}Ge_{0.8}$ sample was grown at (120 ± 20) °C by Ar^+ ion-assisted molecular beam epitaxy with ion energy of ~50 eV. The second sample was a 250 Å alloy of α-$Sn_{0.01}Ge_{0.99}$ thermally grown at (150 ± 20) °C, a temperature sufficiently high so as to result in a small concentration of Sn islands segregated on the surface. For both films, Sn was evaporated from a Knudsen-type effusion cell and Ge from an electron beam evaporator. We did not observe evidence of significant surface oxidation of the SnGe films, presumably because the incidence angle of the electron beam was such that it primarily probed the underlying film. We did not see any EXELFS contribution from thick, three-dimensional β-Sn islands in the second sample. This can be understood by considering that the Debye temperature of β-Sn is ~200 K, so that the room temperature thermal vibration amplitude would greatly reduce the β-Sn contribution to the EXELFS.

The EXELFS oscillations obtained from REELS spectra of these alloys are shown in Fig. 5, and the Fourier transforms of these $\chi(k)$ functions are shown in Fig. 6. The Sn in

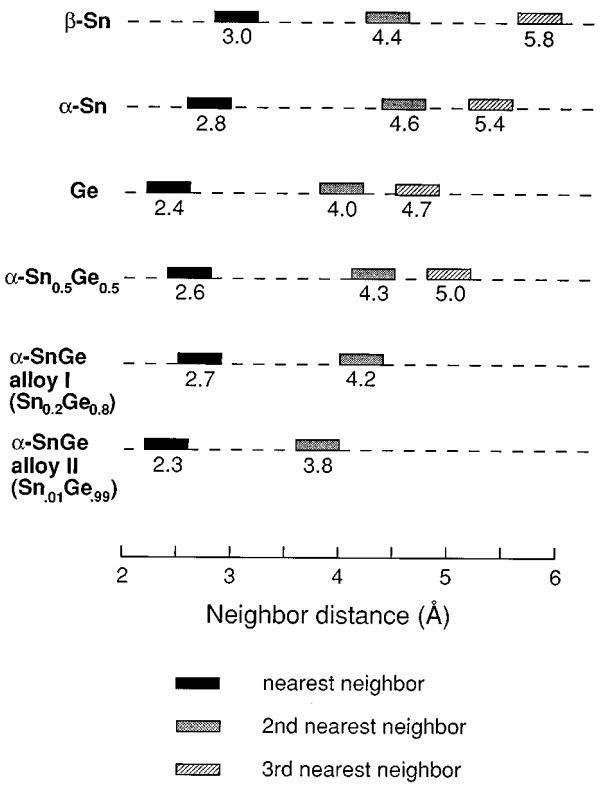

FIG. 7. Nearest-neighbor distances of α-SnGe alloys I and II in this work, along with expected nearest-neighbor separations in α-Sn, α-Ge, β-Sn, and α-$Sn_{0.5}Ge_{0.5}$ in accordance with the virtual crystal approximation.

both alloys has a high probability of having Ge first-nearest neighbors in tetrahedral coordination, which is plausible because of the very small Sn concentrations. For the alloy with 20% Sn concentration (α-SnGe alloy I), the Sn atoms may be pictured as being surrounded by mostly Ge atoms, but with a Sn–Ge bond distance slightly larger than the Ge–Ge distance, which is expected, due to the larger Sn concentration in this strain-relieved epitaxial alloy. We found a Sn–Ge distance of (2.7 ± 0.2) Å. For the alloy with 1% Sn concentration (α-SnGe alloy II), we found a Sn–Ge distance of (2.4 ± 0.2) Å. For both samples, the distances of second- as well as first-nearest neighbors are in agreement with our model of Sn atom surroundings in dilute SnGe alloys. We have encapsulated our experimental findings of nearest-neighbor distances, along with expected nearest-neighbor distances for α-Sn, α-Ge, β-Sn, and α-$Sn_{0.5}Ge_{0.5}$ in accordance with the virtual crystal approximation, in Fig. 7.

V. CONCLUSIONS

REELS EXELFS has been demonstrated for monolayer Sn films, epitaxial SnGe thin film alloys, and Si(100) surfaces. The first- and second-nearest neighbor distances in single crystals are consistent with previous transmission EXELFS and EXAFS data, and we found that first- and second-nearest neighbor distances in SnGe alloys increase with Sn composition. REELS EXELFS is more difficult than transmission EXELFS due to effects of multiple inelastic scattering in the reflection geometry; however, the data rates obtained are comparable to those of synchrotron surface EXAFS measurements and might be higher with parallel detection.

REELS EXELFS has been shown to be complementary to RHEED and REELS, allowing surface science measurements of long-range order (RHEED), long-range composition (REELS), and short-range order (EXELFS) to be obtained with a conventional RHEED system in a conventional molecular beam epitaxy growth system.

ACKNOWLEDGMENT

This work was supported by the National Science Foundation (DMR-9202587).

[1] R. L. Headrick *et al.*, J. Cryst. Growth **111**, 838 (1991).
[2] See, for example, M. E. Hoenk, P. J. Grunthaner, F. J. Grunthaner, R. W. Terhune, M. Fattahi, and H.-F. Tseng, Appl. Phys. Lett. **61**, 1084 (1992).
[3] S. Iwanari and K. Takayanagi, Jpn. J. Appl. Phys. **30**, 1978 (1991).
[4] S. Adachi, J. Appl. Phys. **66**, 813 (1989).
[5] G. He and H. A. Atwater, J. Vac. Sci. Technol. (submitted).
[6] T. Tylisczak, M. de Crescenzi, and A. P. Hitchcock, Phys. Rev. B **37**, 664 (1988).
[7] H. A. Atwater and C. C. Ahn, Appl. Phys. Lett. **58**, 269 (1991).
[8] S. S. Wong, S. Nikzad, C. C. Ahn, A. L. Smith, and H. A. Atwater, Mater. Res. Soc. Symp. Proc. **259**, 449 (1992).
[9] S. Nikzad, C. C. Ahn, and H. A. Atwater, J. Vac. Sci. Technol. B **10**, 762 (1992).
[10] M. de Crescenzi, J. Vac. Sci. Technol. A **5**, 869 (1987).
[11] K. Ueda, K. Kinoshita, and M. Mannami, Surf. Sci. **145**, 261 (1984).
[12] J. K. Okamoto, Ph.D. thesis, Materials Science Dept., California Institute of Technology, 1993.
[13] M. M. Disko, C. C. Ahn, and B. Fultz, *Transmission Electron Energy Loss Spectrometry in Materials Science* (TMS, Warrendale, PA, 1992).
[14] L. Li, Y. Wei, and I. S. T. Tsong, Surf. Sci. **304**, 1 (1994).